Impacts of stratospheric ozone extremes on Arctic high cloud

by

Sarah Maleska *(University of Toronto Scarborough, Toronto, Ontario, Canada; corresponding author: sarahmaleska@gmail.com)*, Karen L. Smith *(University of Toronto Scarborough, Toronto, Ontario, Canada)*, and John Virgin *(University of Waterloo, Waterloo, Ontario, Canada)*

Early Online Release: This preliminary version has been accepted for publication in *Journal of Climate*, may be fully cited, and has been assigned DOI 10.1175/JCLI-D-19-0867.1. The final typeset copyedited article will replace the EOR at the above DOI when it is published.

Abstract

Stratospheric ozone depletion in the Antarctic is well known to cause changes in Southern Hemisphere tropospheric climate; however, due to its smaller magnitude in the Arctic, the effects of stratospheric ozone depletion on Northern Hemisphere tropospheric climate are not as obvious or well understood. Recent research using both global climate models and observational data has determined that the impact of ozone depletion on ozone extremes can affect interannual variability in tropospheric circulation in the Northern Hemisphere in spring. To further this work, we use a coupled chemistry-climate model to examine the difference in high cloud between years with anomalously low and high Arctic stratospheric ozone concentrations. We find that low ozone extremes during the late twentieth century, when ODS emissions are higher, are related to a decrease in upper tropospheric stability and an increase in high cloud fraction, which may contribute to enhanced Arctic surface warming in spring via a positive long-wave cloud radiative effect . A better understanding of how Arctic climate is affected by ODS emissions, ozone depletion and ozone extremes will lead to improved predictions of Arctic climate and its associated feedbacks with atmospheric fields as ozone levels recover.

Accepted for publication in *Journal of Climate*. DOI10.1175/JCLI-D-19-0867.1.

1 Introduction

Stratospheric ozone depletion has transformed Southern Hemisphere climate since the 1980's. Characterized by a positive trend in the Southern Annular Mode, virtually every component of Southern Hemisphere climate has been influenced by ozone depletion in recent decades (Polvani et al., 2011; Previdi & Polvani, 2014; Thompson et al., 2011). The discovery that ozone depletion high above in the stratosphere can generate a downward-migrating stratosphere-troposphere coupled response has revealed the important role that ozone depletion has played in driving recent multi-decadal trends in Southern Hemisphere surface climate (Lee & Feldstein, 2013; Polvani et al., 2011; World Meteorological Organization, 2014). Conversely, the Northern Hemisphere has experienced less ozone depletion due to climatologically greater planetary wave driving. This helps to maintain warmer lower stratospheric temperatures in the Arctic, temperatures that are often above the 192 K temperature threshold needed to form polar stratospheric clouds, which are essential for facilitating the heterogeneous chemical reactions involved in ozone depletion (Solomon et al., 1986). Despite weaker long-term negative trends in stratospheric ozone in the Arctic relative to the Antarctic, recent studies have identified an increase in frequency of extreme low ozone events in spring in the Arctic and have linked these events to changes in Northern Hemisphere tropospheric and surface climate (Calvo et al., 2015; Ivy et al., 2017; Manney et al., 2011; Smith & Polvani, 2014; Xia et al., 2018; Zhang et al., 2018). These low ozone extremes are dynamically initiated and subsequently enhanced by chemical ozone loss and chemistry-climate feedbacks (Calvo et al. 2015). Here, we expand on this work and investigate the role of Arctic ozone depletion on high cloud formation using an ensemble of global climate model (GCM) integrations.

Accepted for publication in *Journal of Climate*. DOI10.1175/JCLI-D-19-0867.1.

Ozone depletion occurs primarily within the cold stratospheric polar vortex (SPV) in spring, when daylight returns to the poles. Sufficiently cold stratospheric conditions combined with ultraviolet radiation provide ideal conditions for ozone-depleting photolytic chemical reactions to occur. Thus, studies examining the effects of ozone extremes on climate have focused on springtime events and the subsequent climate response. In the Southern Hemisphere, springtime Antarctic ozone depletion, i.e. from September to November, has resulted in the most significant climate response in austral summer, December to February. In the Northern Hemisphere, Arctic ozone depletion peaks in March-April and past research has identified significant climate impacts in April-May (Calvo et al., 2015).

Using the Community Atmosphere Model version 3 (CAM3), a climate model with a coarse representation of stratospheric circulation and no interactive stratospheric chemistry, Smith & Polvani (2014) compare 100-year long GCM integrations with prescribed low or high springtime ozone. The prescribed ozone forcings were zonally symmetric, with magnitudes of +/- 15% and +/- 25% relative to climatology (15% is within recently observed ozone variability whereas 25% is slightly larger) for a total of four 100-year long integrations. Comparing the integrations with the 25% lower and higher ozone forcings, the authors find significant differences in tropospheric circulation, surface temperatures, and precipitation patterns, which resemble circulation anomalies typically observed during the positive phase of the Northern Annular Mode (NAM), the leading mode of variability in the northern extratropical atmosphere. This NAM response is characteristic of a dynamically coupled stratosphere-troposphere response, such that anomalies in the stratosphere migrate downward and project onto the leading mode of variability in the troposphere.

Accepted for publication in *Journal of Climate*. DOI10.1175/JCLI-D-19-0867.1.

Conversely, for the more realistic +/- 15% ozone forcings, the atmospheric response in CAM3 is limited to the stratosphere and no statistically significant tropospheric response is detected. This study demonstrates that large Arctic ozone anomalies have the potential to influence Northern Hemisphere circulation, but the study is limited by the fact that the ozone forcing is prescribed and that it is a simple zonal mean quantity.

A subsequent study by Calvo et al. (2015) uses a coupled chemistry-climate model, the Whole Atmosphere Community Climate Model version 4 (WACCM4), to compare extreme high and low ozone years during the second half of the twentieth century. The key differences between WACCM4 and CAM3, used in the Smith & Polvani, (2014) study, are that WACCM4 has a much better resolved stratospheric circulation and includes interactive middle atmosphere chemistry (Marsh et al., 2013). Thus, ozone in WACCM4 is fully coupled and consistent with the model dynamics. With an ensemble of six historical integrations, the authors analyze how April stratospheric ozone concentrationss affect April-May climate. Specifically, they examine composite differences in years with low and high spring ozone during two time periods, the 1955-1975 time period, when ozone depletion is minimal, and the 1985-2005 time period, when ozone depletion is more pronounced. Like Smith & Polvani (2014), Calvo et al. (2015) find the SLP composite mean difference between the low and high ozone years resembles the positive phase of the NAM during the time period with enhanced ozone depletion (1985-2005), but that the difference is statistically insignificant during the time period with less ozone depletion (1955-1975). Most notably, they show that Arctic ozone extremes in WACCM4, computed interactively using *observed* emissions of ozone-depleting substances (ODS), can result in statistically significant anomalies in tropospheric winds, surface temperature, and precipitation

Accepted for publication in *Journal of Climate*. DOI10.1175/JCLI-D-19-0867.1.

over large regions of the Northern Hemisphere without artificially manipulating ozone concentrations.

The above modelling studies are supported by recent observational analysis. Ivy et al. (2017) use satellite-derived ozone observations and a reanalysis data product to examine the relationship between March Arctic ozone anomalies and March-April average tropospheric circulation and surface climate. Like the above studies, they also find an association between negative ozone anomalies in March, a stronger polar vortex, and the positive phase of the NAM in spring. The study also finds that ozone depletion is associated with significant surface warming in most regions north of 70°N, with northern Eurasia having the largest surface temperature anomaly of more than 5 K.

Given the observational and modelling evidence for a connection between Arctic ozone extremes and tropospheric circulation, it is of interest to further investigate whether other aspects of tropospheric climate are influenced by ozone extremes. In the present study, we focus on the impact of ozone extremes on cloud incidence using a coupled chemistry-climate model. High clouds are of particular interest due to their tendency to act as a greenhouse gas, trapping longwave radiation in the atmosphere and re-emitting it back to the Earth's surface, increasing its surface temperature. Recent modelling work by Polvani et al. (2020) suggests that ODS emissions and ozone depletion have resulted in a positive Arctic long-wave cloud radiative adjustment and/or feedback, enhancing Arctic Amplification, the accelerated surface warming in the Arctic, over the past several decades. Xia et al. (2016, 2018) also find that changes in stratospheric ozone significantly affect global high cloud fraction, and consequently the effective

Accepted for publication in *Journal of Climate*. DOI10.1175/JCLI-D-19-0867.1.

radiative forcing of stratospheric ozone perturbations (Shindell et al. 2013, Checa-Garcia et al. 2018).

Following the method of Calvo et al. (2015), we show that low ozone extremes during the late twentieth century are associated with significant positive anomalies in Arctic high cloud, with the largest magnitude anomalies occuring over northern Eurasia. While most of this increase is consistent with large-scale dynamical processes associated with the positive phase of the NAM, as much as half of the high cloud increase over the Kara and Laptev Seas is not, suggesting a potential role for direct, local rapid adjustment. This work contributes to a clearer understanding of how Arctic high cloud incidence is related to stratospheric ozone, and may help to elucidate important dynamical and radiative adjustments or feedbacks associated with ozone depletion in recent decades.

2 Data and Analysis

2.1 Model Data

We analyze six historical integrations of the Whole Atmosphere Community Climate Model version 4 (WACCM4), part of NCAR's Community Earth System Model version 1 (CESM1), from 1955-2005 (Marsh et al., 2013). A superset of the Community Atmosphere Model version 4 (CAM4), WACCM4 (hereafter, simply WACCM) is a chemistry-climate model that extends from the Earth's surface to the lower thermosphere (140 km) with a total of 66 vertical pressure levels and is fully coupled to ocean, land, and sea ice components. It has a horizontal resolution of 1.9° latitude by 2.5° longitude. The model is suitable for analyzing stratosphere-troposphere interactions and can simulate the development of the ozone hole in good agreement with observations (Marsh et al., 2013). Additionally, WACCM's parameterization of nonorographic

Accepted for publication in *Journal of Climate*. DOI10.1175/JCLI-D-19-0867.1.

gravity waves and surface stress due to unresolved topography has improved the representation of SSWs compared to its predecessors, which is especially important for the simulation of stratosphere-troposphere interactions (Garcia et al., 2007; Marsh et al., 2013; Richter et al., 2010).

2.2 Analysis

2.2.1 Low-High Ozone Years

To isolate the effects of ozone depletion and minimize the effects of climate change on the selected fields, Calvo et al.'s (2015) method of separating low ozone and high ozone years was employed. Early (1955-1975) and late (1985-2005) period ozone levels were evaluated at 72 hPa (lower stratosphere) in April. The 30 lowest and 30 highest ozone years were selected from a subset of 126 years for each period (21 years per period multiplied by 6 runs) by polar cap averaging ozone (between 65N and 90N) at 72 hPa and determining the years which had the 30 minimum and 30 maximum polar cap ozone levels in April. To evaluate how ozone extremes affect the various atmospheric fields, the 30 highest and 30 lowest ozone years were used to generate composites of the fields, then the difference was taken between low and high ozone composite means resulting in a 'low-high' anomaly pattern for each field in the early and late periods. Hereafter, we will refer to the low minus high ozone years anomaly pattern as the low-high anomaly pattern for simplicity. The April-May average was taken for each field as in Calvo et al. (2015).

2.2.2 Projections onto the Northern Annular Mode

Previous studies have demonstrated that ozone depletion is associated with rapid adjustments and/or feedbacks in high cloud (Xia et al. 2016, 2018, Virgin & Smith, 2019, Polvani et al.

Accepted for publication in *Journal of Climate*. DOI10.1175/JCLI-D-19-0867.1.

2020); however, the extent to which such adjustments and/or feedbacks exist for *seasonal* Arctic ozone extremes and the mechanisms involved are unclear. Here, we apply the conceptual framework of the fluctuation-dissipation theorem, whereby a dynamical system's response to a perturbation projects onto its leading mode of variability, to qualitatively assess the relative importance of large-scale dynamics and local dynamical and/or radiative adjustments associated with Arctic ozone extremes on high cloud..

As in previous studies, we are interested in the extent to which a response or anomaly pattern (in our case, the low-high anomaly pattern) resembles the leading mode of variability in its natural, unforced state (Deser et al. 2004, McKenna et al. 2018). This has been previously identified as the "indirect" component of the anomaly. The difference between the total anomaly and the indirect component, i.e., the residual, has been identified at the "direct" or forced component and tends to be localized to the forcing region.

In Deser et al. (2004) and McKenna et al. (2018), a companion control model integration is used to establish the unforced leading mode of variability. In the present study, we use the NAM index from the early period (1955-1975) to represent variability that is unforced by ozone depletion. We compute the NAM index using April-May sea level pressure (SLP) from 20°N to 90°N. We then regress each tropospheric and surface field of interest, again for the early period,onto the NAM index (126 years each) to obtain its unforced NAM-associated spatial anomaly pattern. For example, for high cloud, we regress early period high cloud onto the early period NAM index to obtain the spatial pattern of anomalous high cloud associated with the NAM.

Accepted for publication in *Journal of Climate*. DOI10.1175/JCLI-D-19-0867.1.

Next, we compare our anomalies for each extreme ozone year to the above unforced NAM-associated spatial anomaly pattern. To do this, we generate spatial anomalies for each ozone year by removing the climatology for a given field for each of the early and late periods separately. We then project these spatial anomalies against the unforced NAM-associated spatial anomaly pattern for the early period using least-squares regression following Deser et al. (2004) and McKenna et al. (2018). To calculate the residual, the component of the total anomaly that does not project onto the NAM, the projection is subtracted from the total low-high anomaly pattern.

Lastly, for both the NAM projection and the residual components, we calculate the composite mean of each of the 30 years of anomalies (for each of the early and late, low and high ozone years) and take the difference between low and high ozone year composites for each early and late period.

For stratospheric fields, namely stratospheric ozone, we perform a similar decomposition using a NAM index calculated using April geopotential height at 72 hPa.

2.2.3 Upper Tropospheric Stability

Atmospheric stability can be used as an indicator of cloud formation (unstable, rising air is more likely to result in cloud formation, see Li et al. (2014b) for a detailed observational analysis linking cloud incidence, atmospheric stability, and vertical motion). Therefore, we calculated atmospheric static stability for the upper tropospheric region between 400 hPa and the tropopause (known as upper tropospheric stability, (UTS)) as a dynamical indicator of high cloud formation:

$$(1) \quad UTS = \theta_{tropopause} - \theta_{400\ hPa}$$

Accepted for publication in *Journal of Climate*. DOI10.1175/JCLI-D-19-0867.1.

(Klein & Hartmann, 1993; Li et al., 2014b). Note that our analysis is not sensitive to the choice of 400 hPa in our definition of UTS. Pressure levels ranging from 300 to 550 hPa yield similar results.

2.2.4 Cloud Feedback Calculation

We approximate the cloud feedback using the adjusted Cloud Radiative Effect (CRE) method (Soden et al. 2008). The *CRE* is defined as the difference between top-of-atmosphere (TOA) radiative fluxes between clear- and total-sky conditions, or:

$$(2) \quad CRE = R(T, q, 0, a) - R(T, q, c, a)$$

Where *T*, *q*, *c*, *0*, *a*, denote temperature, water vapour, total-sky cloud, clear-sky cloud, and albedo, respectively, and *R* represents the net radiative flux at the TOA. The cloud feedback is calculated by adjusting the anomaly in *CRE*, *dCRE*, as follows:

$$(3) \quad \lambda_c = dCRE + (K_T^0 - K_T)dT + \left(K_q^0 - K_q\right)dq + (K_a^0 - K_a)da + (Fo - F)$$

where *dT*, *dq*, and *da* represent the anomalies in *T*, *q* and *a*, *K* represents the radiative kernel associated with a given feedback (we use the CAM3 kernels; Shell et al., 2008), *F* denotes the radiative forcing and superscript 0 denotes clear-sky. For the long-wave cloud feedback associated with ozone depletion, we can neglect the albedo term and we assume that the difference in total-sky and clear-sky radiative forcing is negligible.

Accepted for publication in *Journal of Climate*. DOI10.1175/JCLI-D-19-0867.1.

2.2.5 Significance Testing and Regression

To determine the statistical significance of the composite mean low-high anomaly patterns, we use a 2-sample Student's t-test to identify regions of statistically significant differences at the 95% confidence level.

We also use least-squares linear regression to explore the relationships between high cloud, UTS, and ozone concentration for low and high ozone years in both the early and late periods.

3 Results

While ozone depletion is substantially less in the Arctic than it is in the Antarctic, it is nevertheless significant. Due to large dynamically-driven variability in the Arctic lower stratosphere, Arctic ozone depletion is most evident when we contrast springtime ozone extremes. To demonstrate this, we first show how Arctic ozone extremes evolve in WACCM between the early and late time periods. The WACCM ensemble mean April ozone concentration in mol ozone per mol air at 72 hPa for the 30 highest and lowest ozone years in the early and late periods is presented in Figure 1. Ozone values range from 1.16×10^{-6} mol O_3/mol air during the late period's lowest ozone years, to 3.26×10^{-6} mol O_3/mol air during the early period's highest ozone years. Of particular interest is the similarity of the ensemble mean low ozone pattern and magnitude in the early period to the ensemble mean high ozone in the late period (Figs. 1b, c). This is indicative of the dramatic effect that ozone depleting substances (ODS's) have had on ozone in the Arctic stratosphere. Also of note is that the ozone minimum in the late period is skewed towards northern Eurasia – a spatial feature that will appear throughout our analysis.

Accepted for publication in *Journal of Climate*. DOI10.1175/JCLI-D-19-0867.1.

To further elucidate the magnitude of the ozone anomaly, the low-high anomaly in April ozone for the early and late periods is shown in Figure 2 as well as how much of that anomaly projects onto the NAM and how much does not. Comparing the early and late total low-high ozone anomaly in Figs. 2a and 2d highlights the enhanced chemical ozone depletion in the late period compared to the early period; the total low-high anomaly in ozone in the late period is about two times larger than that of the early period.

Figures 2b and 2e show the projection of the low-high ozone anomaly onto the April NAM index at 72 hPa. The stratospheric NAM projection serves to elucidate the processes driving ozone extremes. The component of the total low-high ozone anomaly that projects onto the NAM represents the fraction associated with large-scale dynamical transport. For the late period, this also includes any decrease in transport associated with chemistry-climate feedbacks related to chemical ozone loss. In the early period, dynamical transport accounts for much of the total low-high ozone anomaly (Fig. 2b). However, in the late period, we find that both the NAM-projection (Fig. 2e) and the residual (Fig. 2f) components are substantial, particularly over the eastern Arctic. The residual is the portion of the total anomaly that is not consistent with the NAM and therefore represents more of a direct and local forced response to ODS emissions. We find that approximately half of the total ozone anomaly over the eastern Arctic is explained by processes that are not dynamically consistent with the NAM. This decomposition highlights the very different nature of low ozone years at the end of the twentieth century – rather than being primarily associated with reduced dynamical ozone transport (Tegtmeier et al., 2008), they are also associated with substantial chemical loss.

Accepted for publication in *Journal of Climate*. DOI10.1175/JCLI-D-19-0867.1.

Before proceeding to the analysis of cloud incidence, we first reproduce the low-high anomaly in SLP shown in Calvo et al. (2015). Figures 3a and 3d show the total SLP anomalies for the early and late periods, respectively. As in Calvo et al. (2015), we see a statistically significant SLP anomaly resembling the positive phase of the NAM for the late period, but not for the early period. Unlike stratospheric ozone (Fig. 2), the total SLP anomaly is almost entirely explained by its projection onto the NAM. This suggests that although we see a clear signal of forced chemical ozone loss in the residual in Figure 2f, the low-high anomaly in the tropospheric circulation in Figure 3e reflects an indirect large-scale dynamical stratosphere-troposphere coupled response to ozone loss that projects almost entirely onto the NAM. This agrees with idealized modelling studies, such as Kushner and Polvani (2004) and Simpson et al., (2009) which show that polar stratospheric forcings can elicit an equivalent barotropic NAM-like tropospheric circulation response via tropospheric eddy feedbacks. .

Previous studies have shown that the positive phase of the NAM is associated with increased high cloud incidence north of ~ 60°N (Li et al., 2014a; Previdi & Veron, 2007). Thus, based on the projection of the low-high anomaly in SLP onto the positive phase of the NAM in Figure 3e, we anticipate an accompanying positive anomaly in high cloud over the Arctic region. This is indeed what we find in WACCM. Figure 4 shows the zonal mean low-high total cloud fraction anomaly for the early and late periods. The anomaly is small and not significant north of 60°N for the early period (Fig. 4a), but the late period shows a significant positive anomaly in cloud fraction, particularly high cloud, north of 70°N (Fig. 4b). For the late period, we also see significant high cloud fraction anomalies for both the NAM-projected (Fig. 4d) and residual (Fig. 4f) components during the late period.

Accepted for publication in *Journal of Climate*. DOI10.1175/JCLI-D-19-0867.1.

Isolating the high cloud component, Figure 5 shows the total low-high anomaly in high cloud, how much of that anomaly projects onto the NAM, and the residual for the early and late periods. There is no significant difference in high cloud fraction between low and high ozone years for the early period over the Arctic (Figure 5a), whereas there is a significant positive anomaly in Arctic high cloud in the late period, especially over the eastern Arctic and northern Eurasia (Figure 5d). Similarly, the projected and residual components show no significant difference in high cloud in the early period (Figs. 5b, c) whereas there are significant positive anomalies in high cloud over the pole in the late period (Figs. 5e, f). The late period NAM-projected positive anomaly in high cloud covers almost the entire pole, except for a small area over southwest Greenland, thus linking the majority of the total high cloud anomaly to ozone extremes associated with ozone depletion via large-scale atmospheric circulation. For the late period residual, smaller areas of positive high cloud anomalies are also significant, particularly over the Kara and Laptev Seas and Greenland, as well as bands of negative high cloud anomalies over northern Asia, northeastern Canada, and the northeastern Atlantic. The polar cap-averaged Arctic high cloud anomaly for the late period is 5.3%, with 3.8% associated with the NAM and 1.5% remaining.

One of the proposed mechanisms linking Arctic high cloud incidence to the NAM is via the dynamical coupling between the stratosphere and troposphere. Anomalies in Arctic high cloud have been associated with variability in stratospheric wave driving and the consequent anomalies in near-tropopause temperature (Li & Thompson, 2013); specifically, Li et al. (2014b) identify a link between decreased tropopause temperature and increased upper tropospheric high clouds in the Arctic. In what follows, we examine whether anomalously cold near-tropopause temperatures associated with stratospheric ozone extremes in the Arctic can be similarly linked

Accepted for publication in *Journal of Climate*. DOI10.1175/JCLI-D-19-0867.1.

to anomalously positive high cloud fraction. Figure 6 shows the zonal mean difference in potential temperature between low and high ozone years for the early and late periods. We show potential temperature rather than temperature to allow for ease of comparison with UTS (see Figure 7). Also included is the tropopause pressure for low and high ozone years for each period and the average tropopause temperature. Both periods experience significant anomalies in stratospheric potential temperature (Figs. 6a, b), but the anomalies in the late period are larger in magnitude and occur just above the tropopause, at around ~80 hPa, while the anomalies in the early period are weaker and occur at a higher altitude. This is consistent with what is already known about the relationship between ozone depletion, tropopause temperature/height, and lower stratospheric temperature (McLandress et al., 2011; Polvani et al., 2011). As expected, for the late period low ozone years, the lower stratosphere cools and the tropopause rises. The tropopause temperature also decreases by 1.07 K in the late period (compared to a decrease of only 0.17 K between low and high ozone years in the early period). For the late period we also find significant anomalies in zonal mean potential temperature for both the NAM-projected (Fig. 6d) and residual (Fig. 6f) components. The differing vertical structure of these potential temperature anomalies qualitatively distinguishes between dynamically-driven anomalies and radiatively-driven anomalies, respectively.

Because low ozone extremes associated with chemical ozone depletion in the late period cause greater stratospheric cooling, specifically in the lower stratosphere and upper troposphere, a potential physical link may be made between ozone depletion and enhanced high cloud incidence in the Arctic via a decrease in upper tropospheric stability (UTS). Figure 7 shows the total, NAM-projected, and residual UTS for the early and late periods. Although we find that the total low-high anomaly in UTS is negative in both the early and late period, we find much larger

Accepted for publication in *Journal of Climate*. DOI10.1175/JCLI-D-19-0867.1.

magnitude anomalies in the late period. The significant negative anomaly in total UTS over the eastern Arctic and northern Eurasia in the late period is notable. A similar pattern was found in both the ozone anomaly (Figure 2d) and the high cloud anomaly (Figure 5d), again suggesting a link between ozone, UTS, and high cloud anomalies. We will examine this region (outlined in red in Figure 7a) in greater detail in Figure 8.

As we have seen for high cloud, most of the negative anomaly in UTS over the eastern Arctic and northern Eurasia is consistent with its projection onto the NAM (compare Figure 7e and Figure 5e); however, a small, but significant part of the negative anomaly is found in the residual (compare Figure 7f and Figure 5f).

Based on the composite analysis thus far, we have identified significant differences in low-high anomalies in ozone, UTS, and high cloud during the period when chemical ozone depletion is significant, suggesting a mechanistic physical connection between ozone depletion and high cloud anomalies. Additionally, we find that a large part of each total anomaly pattern (except ozone) can be explained by its projection onto the NAM. We interpret our NAM-projection analysis as largely supporting previous work that argues for a dynamically coupled stratosphere-troposphere response to Arctic ozone depletion (Smith and Polvani, 2014; Calvo et al., 2015; Ivy et al., 2017). However, the residual in our low-high anomalies in UTS and high cloud suggest that there may be other local dynamical or radiative processes that contribute to the total anomaly patterns, , particularly in Laptev and Kara Seas region.

We now examine these results further using regression analysis for individual low/high, early/late ozone years, to gain a better understanding of the processes contributing to positive high cloud anomalies in the presence of ozone depletion. Figure 8 contains seven scatter plots

Accepted for publication in *Journal of Climate*. DOI10.1175/JCLI-D-19-0867.1.

illustrating the linear relationships between anomalies in April ozone (total, NAM-projected, and residual) and April-May total UTS and high cloud for the northern Eurasia region as outlined in red in Figure 7d (the results are qualitatively similar for the Arctic region). In Figure 8a, UTS is regressed against high cloud fraction. The four early/late, low/high combinations are significantly negatively correlated supporting previous work (Li et al. 2013, 2014b); the late, low ozone combination has the lowest UTS and highest high cloud values. UTS is then regressed against total ozone in Figure 8b. Notice that the early low and high, and late high ozone years cluster together in the plot, while the late low ozone years are clearly separated. This separation yields the composite mean differences shown in Figures 2, 5, and 7. Within each grouping, we see that UTS and ozone are positively and significantly correlated with each other, with the exception of the late, high ozone years, demonstrating a robust link between these two fields. Finally, in Figure 8c high cloud is regressed against total ozone. High cloud and ozone are negatively correlated – as ozone levels decrease, high cloud increases and vice versa. The late, low ozone years are again clearly separated from the other years.

In Figures 8d,e and 8f,g we explore the extent to which the nature of the ozone forcing affects the relationships between ozone, UTS, and high cloud over northern Eurasia. Figure 8d,e shows the relationship between NAM-projected ozone, total high cloud, and total UTS. For the late period, low ozone years, the relationships for both high cloud and UTS with NAM-projected ozone are insignificant, while the other groups of years all show statistically significant relationships. In Figure 8f, the residual ozone is significantly positively correlated with UTS for the late low ozone years, but the relationships with high cloud is less clear (Fig. 8g). We find stronger correlations with residual ozone for the low ozone years compared to the high ozone years, a feature that requires further examination. Overall, this analysis demonstrates that the

Accepted for publication in *Journal of Climate*. DOI10.1175/JCLI-D-19-0867.1.

relationships between ozone, UTS and high cloud are robust, but that mechanisms driving these relationships can differ. The strength and significance of the correlations in Figure 8 suggest that ozone extremes that are influenced by large-scale dynamical transport, i.e. the NAM-projected ozone, appear to play an important role in determining anomalies in UTS and high cloud in the early period (Figs. 8d, e), but ozone anomalies that are associated with chemical loss, i.e., the residual ozone, also appear to play an important role in the late period (Figs. 8f).

We have shown using both composite analysis and regression that positive high cloud anomalies in the Arctic are linked to ozone extremes via its effect on upper tropospheric stability. We now ask whether these cloud anomalies could have a radiative influence on surface temperature. In order to answer this question, we examine top-of-atmosphere (TOA) longwave (LW) fluxes associated with high clouds using the adjusted Cloud Radiative Effect (CRE) method (Soden et al., 2008). Figure 9 shows the total, NAM-projected, and residual low-high anomaly in TOA LW adjusted CRE for the early and late periods. The spatial patterns in Figure 9 are strikingly similar to those for high cloud in Figure 5. Overall, the LW warming effect from Arctic cloud is substantially larger in the late period (Fig. 9d) compared to the early period (Fig. 9a), particularly over the eastern Arctic and northern Eurasia, suggesting that the effect of ozone depletion on ozone extremes has the potential to impact surface temperature. As shown previously, much of the anomaly in Arctic high cloud in the late period is associated with the large-scale stratosphere-troposphere coupled NAM response to ozone extremes (Fig. 5e), and this is what we also find for the TOA LW adjusted CRE anomaly (Fig. 9e). This is consistent with the work of Li et al. (2014a) who find that the positive phase of the NAM is associated with positive high cloud anomalies and a positive TOA adjusted CRE in the Arctic region. The late period residual (Fig.

Accepted for publication in *Journal of Climate*. DOI10.1175/JCLI-D-19-0867.1.

9f) shows a significant positive region over the Laptev and Kara Seas, similar to the residual for high cloud (Fig. 5f).

Finally, to further elucidate the effects of ozone extremes on Arctic surface climate, the surface temperature difference between low and high ozone years is shown in Figures 10a and 10d for the early and late periods. The surface temperature pattern was projected onto the early period NAM in Figs. 10b and 10e, indicating how much of the surface temperature pattern is consistent with the large-scale NAM pattern. Then, as before, the residual patterns in Figs. 10c and 10f were calculated by subtracting the projected anomalies from the total. Similar to the positive high cloud, negative UTS and LW adjusted CRE anomalies found mostly over northern Eurasia in Figure 5, 7 and 9, the late period low-high surface temperature anomaly shows a statistically significant warming focused over northern Eurasia (see also Calvo et al. 2015). Most of the positive anomaly in surface temperature in the late period is consistent with the NAM, but there are also regions of significant positive anomalies in surface temperature over Eurasia and the pole in the residual. These regions are approximately spatially co-located with the corresponding residual patterns in ozone, high cloud, UTS and TOA LW adjusted CRE (Figs. 5f, 7f and 9f) and, therefore, potentially represent the warming effect of local rapid adjustments in high cloud associated with ozone extremes (Xia et al. 2016, 2018).

4 Discussion and Conclusions

In this study, we examine the relationship between twentieth century stratospheric ozone extremes and Arctic high cloud. Using a global climate model with interactive stratospheric chemistry, we find that extreme negative Arctic ozone anomalies in spring during the late twentieth century are associated with positive high cloud anomalies in that region.

Accepted for publication in *Journal of Climate*. DOI10.1175/JCLI-D-19-0867.1.

Our work builds on several key studies. First, previous work has demonstrated that springtime ozone extremes in the Arctic results in tropospheric circulation anomalies that project onto the positive phase of the NAM (Calvo et al., 2015; Ivy et al., 2017; Li et al., 2014a; Smith & Polvani, 2014). Second, the positive phase of the NAM has been associated with a positive anomaly in high cloud and cloud radiative effect in the Arctic (Li et al., 2014a). Finally, ozone depletion has been associated with positive rapid adjustments and/or feedbacks in high cloud (Xia et al. 2016, 2018, Virgin & Smith, 2019, Polvani et al. 2020). Taken together, these studies suggest that ozone extremes have the potential to impact Arctic climate via both large-scale dynamical and radiative adjustments and/or feedbacks in high cloud.

Using historical integrations of WACCM, we extend previous work showing that extreme negative springtime Arctic ozone anomalies in the late twentieth century are associated with anomalies in Arctic tropospheric climate by showing a link between ozone extremes and high cloud (Figure 8). During this time period Arctic low ozone extremes are linked to, a rising and cooling of the tropopause (Figure 6), a decrease in upper tropospheric stability (Figure 7), an increase in high cloud fraction (Figure 5), an increase in the TOA adjusted long-wave cloud radiative effect over the Arctic and Eurasia (Figure 9b), and an increase in surface temperature over northern Eurasia (Figure 10). The tropopause rises and cools due to a colder lower stratosphere and the corresponding changes in wave driving (Polvani et al 2011, McLandress et al. 2011). A rising and cooling of the tropopause leads to a decrease in upper tropospheric stability and an increase in high cloud formation (Li & Thompson, 2013). Because high cloud tends to act like a greenhouse gas, this increase in high cloud results in an increase in TOA LW adjusted CRE; however, we cannot make a causal link between the increase in TOA LW adjusted CRE and surface temperature based on the analysis presented.

Accepted for publication in *Journal of Climate*. DOI10.1175/JCLI-D-19-0867.1.

To examine the extent to which our results reflect UTS, high cloud, and surface temperature anomalies associated with large-scale dynamics associated with the NAM or other factors, such as rapid adjustments, we decompose the anomalies into the component that projects onto the NAM and the residual. Consistent with conclusions of previous studies (Calvo et al., 2015; Ivy et al., 2017; Li et al., 2014a; Smith & Polvani, 2014), we find that most of the anomalies in UTS, high cloud, and surface temperature project onto the NAM. However, we do find statistically significant anomalies in the residual that may reflect, in part, the effect of rapid adjustments. This is supported by the fact that the residual anomalies in ozone, UTS, high cloud, and surface temperature are spatially co-located over the northern Eurasian sector of the Arctic.

While the decomposition of anomalies into the NAM-projected component and the residual give some suggestion as to the relative importance of large-scale dynamics versus local rapid adjustments, this decomposition does not provide a clean separation of these mechanisms and our results require further investigation using targeted GCM experiments.

In summary, this work presents a clear link between Arctic springtime ozone extremes and high cloud incidence and, thus, raises questions about the contribution of ozone-induced changes in high cloud on historical Arctic Amplification and how ozone recovery will affect Arctic climate in the coming decades. It is critical to improve our understanding of how stratospheric ozone interacts with climate in order to quantitatively attribute observed climate changes to specific physical and chemical processes, to continually improve climate models, and to reasonably project future climate changes.

Accepted for publication in *Journal of Climate*. DOI10.1175/JCLI-D-19-0867.1.

Acknowledgements

S.M. and K.L.S. gratefully acknowledge support from the Department of Physical and Environmental Sciences at the University of Toronto Scarborough. K. L. S. also acknowledges support from the National Science Foundation (NSF) Division of Polar Programs, PLR-1603350. We also owe tremendous thanks to the National Center for Atmospheric Research (NCAR) and associated supercomputing resources provided by NSF/CISL/Yellowstone. The complete CESM1 (WACCM4) integrations are stored on the NCAR High Performance Storage System. NCAR is sponsored by the NSF.

Accepted for publication in *Journal of Climate*. DOI10.1175/JCLI-D-19-0867.1.

References

Calvo, N., Polvani, L. M., & Solomon, S. (2015). On the surface impact of Arctic stratospheric ozone extremes. *Environmental Research Letters*, *10*(9). https://doi.org/10.1088/1748-9326/10/9/094003

Checa-Garcia, R., Hegglin, M. I., Kinnison, D., Plummer, D. A., & Shine, K. P. (2018). Historical tropospheric and stratospheric ozone radiative forcing using the CMIP6 database. Geophysical Research Letters, 45(7), 3264-3273.

Garcia, R. R., Marsh, D. R., Kinnison, D. E., Boville, B. A., & Sassi, F. (2007). Simulation of secular trends in the middle atmosphere, 1950-2003. *Journal of Geophysical Research Atmospheres*, *112*(9), 1–23. https://doi.org/10.1029/2006JD007485

Ivy, D. J., Solomon, S., Calvo, N., & Thompson, D. W. J. (2017). Observed connections of Arctic stratospheric ozone extremes to Northern Hemisphere surface climate. *Environmental Research Letters*, *12*(2). https://doi.org/10.1088/1748-9326/aa57a4

Klein, S. A., & Hartmann, D. L. (1993). The seasonal cycle of low stratiform clouds. *Journal of Climate*.

Kushner, P. J., & Polvani, L. M. (2004). Stratosphere-Troposphere Coupling in a Relatively Simple AGCM: The Role of Eddies. *Journal of Climate*, *17*(3), 629–639.

Lee, S., & Feldstein, S. B. (2013). Detecting ozone- and greenhouse gas-driven wind trends with observational data. *Science*. https://doi.org/10.1126/science.1225154

Li, Y., & Thompson, D. W. J. (2013). The signature of the stratospheric Brewer-Dobson

Accepted for publication in *Journal of Climate*. DOI10.1175/JCLI-D-19-0867.1.

circulation in tropospheric clouds. *Journal of Geophysical Research Atmospheres*. https://doi.org/10.1002/jgrd.503392013

Li, Y., Thompson, D. W. J., Huang, Y., & Zhang, M. (2014a). Observed linkages between the northern annular mode / North Atlantic Oscillation , cloud incidence , and cloud radiative forcing, 1681–1688. *Geophysical Research Letters*, https://doi.org/10.1002/2013GL059113

Li, Y., Thompson, D. W. J., Stephens, G. L., & Bony, S. (2014b). A global survey of the instantaneous linkages between cloud vertical structure and large-scale climate. *Journal of Geophysical Research*, *119*(7), 3770–3792. https://doi.org/10.1002/2013JD020669

Magnusdottir, G., Deser, C., & Saravanan, R. (2004). The effects of North Atlantic SST and sea ice anomalies on the winter circulation in CCM3. Part I: Main features and storm track characteristics of the response. *Journal of Climate*, *17*(5), 857–876.

Manney, G. L., Santee, M. L., Rex, M., Livesey, N. J., Pitts, M. C., Veefkind, P., … Zinoviev, N. S. (2011). Unprecedented Arctic ozone loss in 2011. *Nature*, *478*(7370), 469–475. https://doi.org/10.1038/nature10556

Marsh, D. R., Mills, M. J., Kinnison, D. E., Lamarque, J. F., Calvo, N., & Polvani, L. M. (2013). Climate change from 1850 to 2005 simulated in CESM1(WACCM). *Journal of Climate*, *26*(19), 7372–7391. https://doi.org/10.1175/JCLI-D-12-00558.1

McKenna, C. M., Bracegirdle, T. J., Shuckburgh, E. F., Haynes, P. H., & Joshi, M. M. (2018). Arctic sea ice loss in different regions leads to contrasting Northern Hemisphere impacts. *Geophysical Research Letters*, 45, 945–954.

https://doi.org/10.1002/2017GL076433McLandress, C., Scinocca, J. F., Shepherd, T. G., Plummer, D. A.,

Accepted for publication in *Journal of Climate*. DOI10.1175/JCLI-D-19-0867.1.

Sigmond, M., Jonsson, A. I., & Reader, M. C. (2011). Separating the Dynamical Effects of Climate Change and Ozone Depletion. Part II: Southern Hemisphere Troposphere. *Journal of Climate*, *24*(6), 1850–1868.

Polvani, L. M., Waugh, D. W., Correa, G. J. P., & Son, S.-W. (2011). Stratospheric Ozone Depletion: The Main Driver of Twentieth-Century Atmospheric Circulation Changes in the Southern Hemisphere. *Journal of Climate*, *24*(3), 795–812. https://doi.org/10.1175/2010JCLI3772.1

Polvani, L. M, M. Previdi, M. England, G. Chiodo and K. L. Smith (2020). Large Arctic warming from ozone depleting substances in the latter half of the 20th Century. *Nature Climate Change*, 10, 130–133. doi:0.1038/s41558-019-0677-4

Previdi, M., & Polvani, L. M. (2014). Climate system response to stratospheric ozone depletion and recovery. *Quarterly Journal of the Royal Meteorological Society*, *140*(685), 2401–2419. https://doi.org/10.1002/qj.2330

Previdi, M., & Veron, D. E. (2007). North Atlantic cloud cover response to the North Atlantic oscillation and relationship to surface temperature changes. *Journal of Geophysical Research*, *112*(D7).

Richter, J. H., Sassi, F., & Garcia, R. R. (2010). Toward a Physically Based Gravity Wave Source Parameterization in a General Circulation Model. *Journal of the Atmospheric Sciences*, *67*(1), 136–156. https://doi.org/10.1175/2009JAS3112.1

Accepted for publication in *Journal of Climate*. DOI10.1175/JCLI-D-19-0867.1.

Shell, K. M., Kiehl, J. T., & Shields, C. A. (2008). Using the radiative kernel technique to calculate climate feedbacks in NCAR's Community Atmospheric Model. *Journal of Climate*, *21*(10), 2269-2282

Shindell, D. T., Pechony, O., Voulgarakis, A., Faluvegi, G., Nazarenko, L., Lamarque, J.-F., Bowman, K., Milly, G., Kovari, B., Ruedy, R., and Schmidt, G. A. (2013). Interactive ozone and methane chemistry in GISS-E2 historical and future climate simulations, Atmos. Chem. Phys., 13, 2653–2689, https://doi.org/10.5194/acp-13-2653-2013.

Simpson, I., Blackburn, M., & Haigh, J. (2009). The Role of Eddies in Driving the Tropospheric Response to Stratospheric Heating Perturbations. *Journal of the Atmospheric Sciences*, *66*(5), 1347–1365.

Smith, K. L., & Polvani, L. M. (2014). The surface impacts of Arctic stratospheric ozone anomalies. *Environmental Research Letters*, *9*(7). https://doi.org/10.1088/1748-9326/9/7/074015

Solomon, S., Garcia, R. R., Rowland, F. S., & Wuebbles, D. J. (1986). On the depletion of Antarctic ozone. *Nature*, *321*(6072), 755–758. https://doi.org/10.1038/321755a0

Tegtmeier, S., Rex, M., Wohltmann, I., & Krüger, K. (2008). Relative importance of dynamical and chemical contributions to Arctic wintertime ozone. *Geophysical Research Letters*, *35*(17), 1–5. https://doi.org/10.1029/2008GL034250

Thompson, D. W. J., Solomon, S., Kushner, P. J., England, M. H., Grise, K. M., & Karoly, D. J. (2011). Signatures of the Antarctic ozone hole in Southern Hemisphere surface climate

Accepted for publication in *Journal of Climate*. DOI10.1175/JCLI-D-19-0867.1.

change. *Nature Geoscience*, *4*(11), 741–749. https://doi.org/10.1038/ngeo1296

Virgin, J., & Smith, K. L. (2019). Is Arctic Amplification Dominated by Regional Radiative Forcing and Feedbacks: Perspectives From the World-Avoided Scenario. *Geophysical Research Letters*, *46*(13), 7708–7717.

World Meteorological Organization (WMO). (2014). *Scientific Assessment of Ozone Depletion: 2014*. *World Meteorological Organization, Global Ozone Research and Monitoring Project - Report No. 55*.

Xia, Y., Hu, Y., and Huang, Y. (2016). Strong modi_cation of stratospheric ozone forcing by cloud and sea-ice adjustments, Atmos. Chem. Phys., 16, 7559{7567, https://doi.org/10.5194/acp-16-7559-2016.

Xia, Y., Huang, Y., & Hu, Y. (2018). On the Climate Impacts of Upper Tropospheric and Lower Stratospheric Ozone. *Journal of Geophysical Research: Atmospheres*, *123*(2), 730–739.

Zhang, J., Tian, W., Xie, F., Chipperfield, M. P., Feng, W., Son, S. W., … Zeng, G. (2018). Stratospheric ozone loss over the Eurasian continent induced by the polar vortex shift. *Nature Communications*, *9*(1), 1–8. https://doi.org/10.1038/s41467-017-02565-2

Accepted for publication in *Journal of Climate*. DOI10.1175/JCLI-D-19-0867.1.

Figures

Accepted for publication in *Journal of Climate*. DOI10.1175/JCLI-D-19-0867.1.

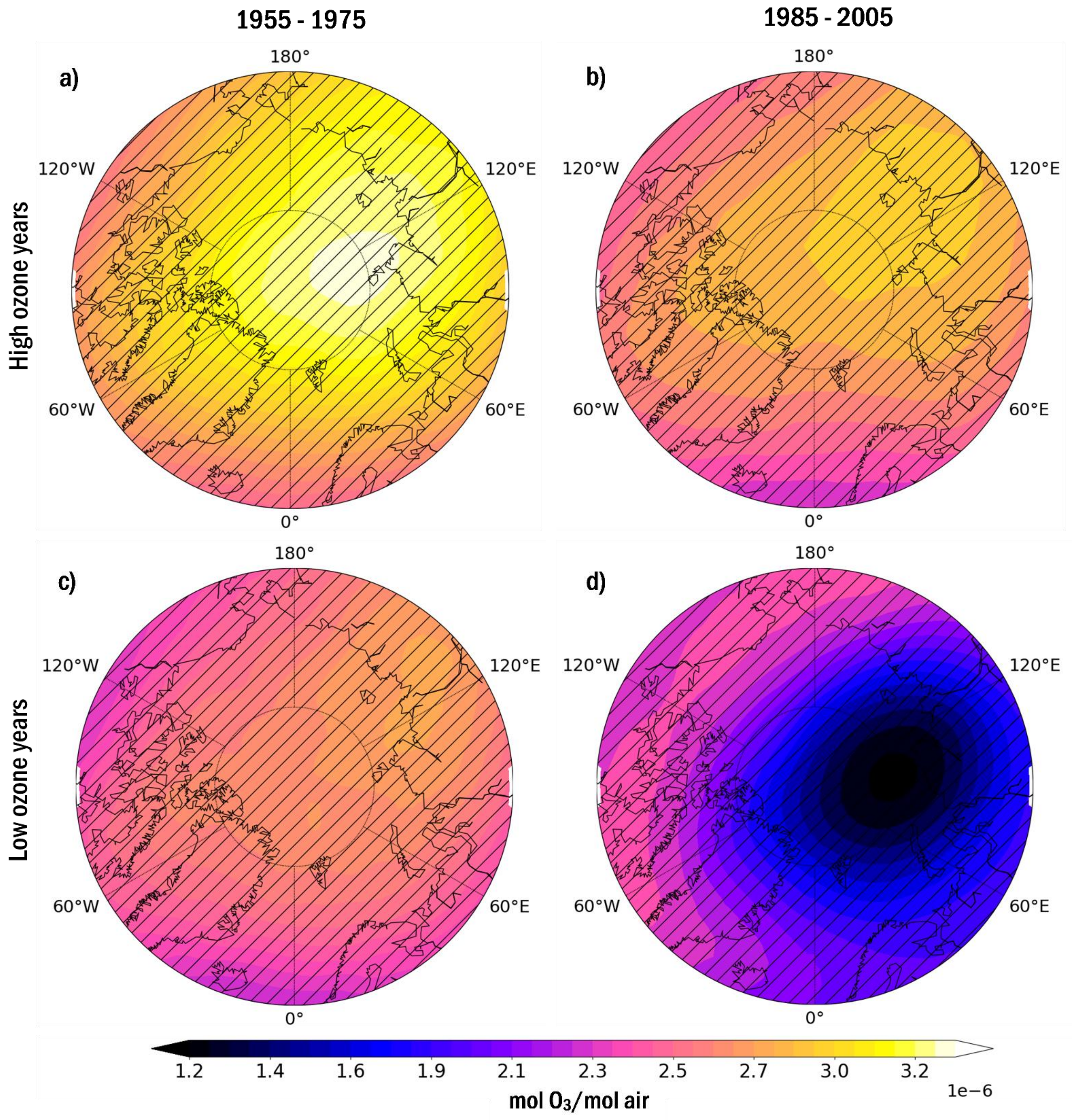

Figure 1. Average April ozone concentration (mol ozone per mol air) for the (top) 30 lowest and (bottom) highest ozone years for the (left) 1955-1975 and (right) 1985-2005 time periods at 72 hPa. Hatching indicates regions of statistical significance at the 95% level.

Accepted for publication in *Journal of Climate*. DOI10.1175/JCLI-D-19-0867.1.

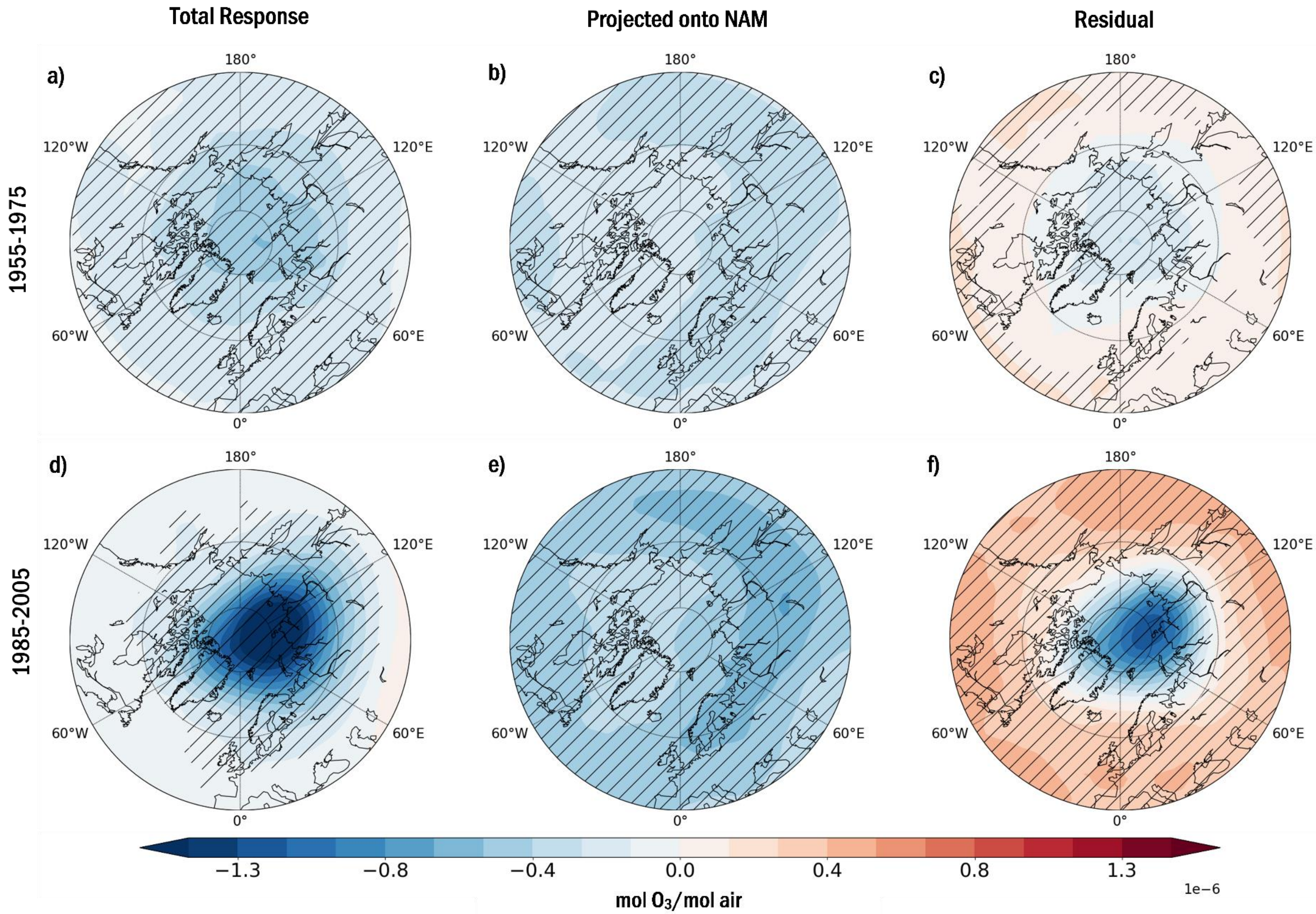

Figure 2. (a), (d) Total April ozone anomaly at 72 hPa (low-high ozone years), (b), (e) the projection of the anomaly onto the NAM, and (c), (f) the residual for the (a)-(c) 1955-1975 and (d)-(f) 1985-2005 time periods. Hatching indicates regions of statistical significance at the 95% level.

Accepted for publication in *Journal of Climate*. DOI10.1175/JCLI-D-19-0867.1.

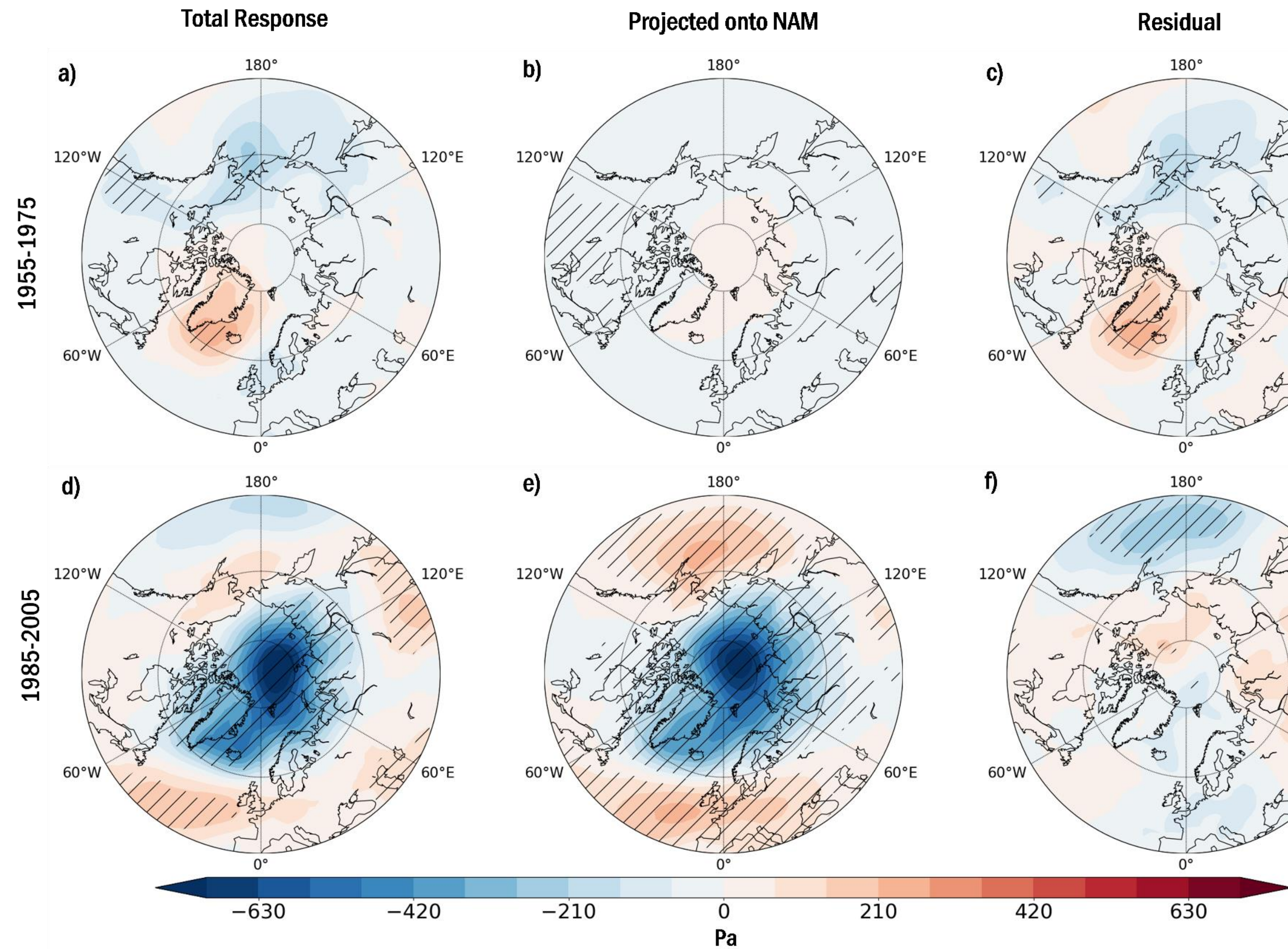

Figure 3. (a), (d) Total April-May SLP anomaly (low – high ozone years), (b), (e) the projection of the anomaly onto the NAM, and (c), (f) the residual for the (a)-(c) 1955-1975 and (d)-(f) 1985-2005 time periods. Hatching indicates regions of statistical significance at the 95% level.

Accepted for publication in *Journal of Climate*. DOI10.1175/JCLI-D-19-0867.1.

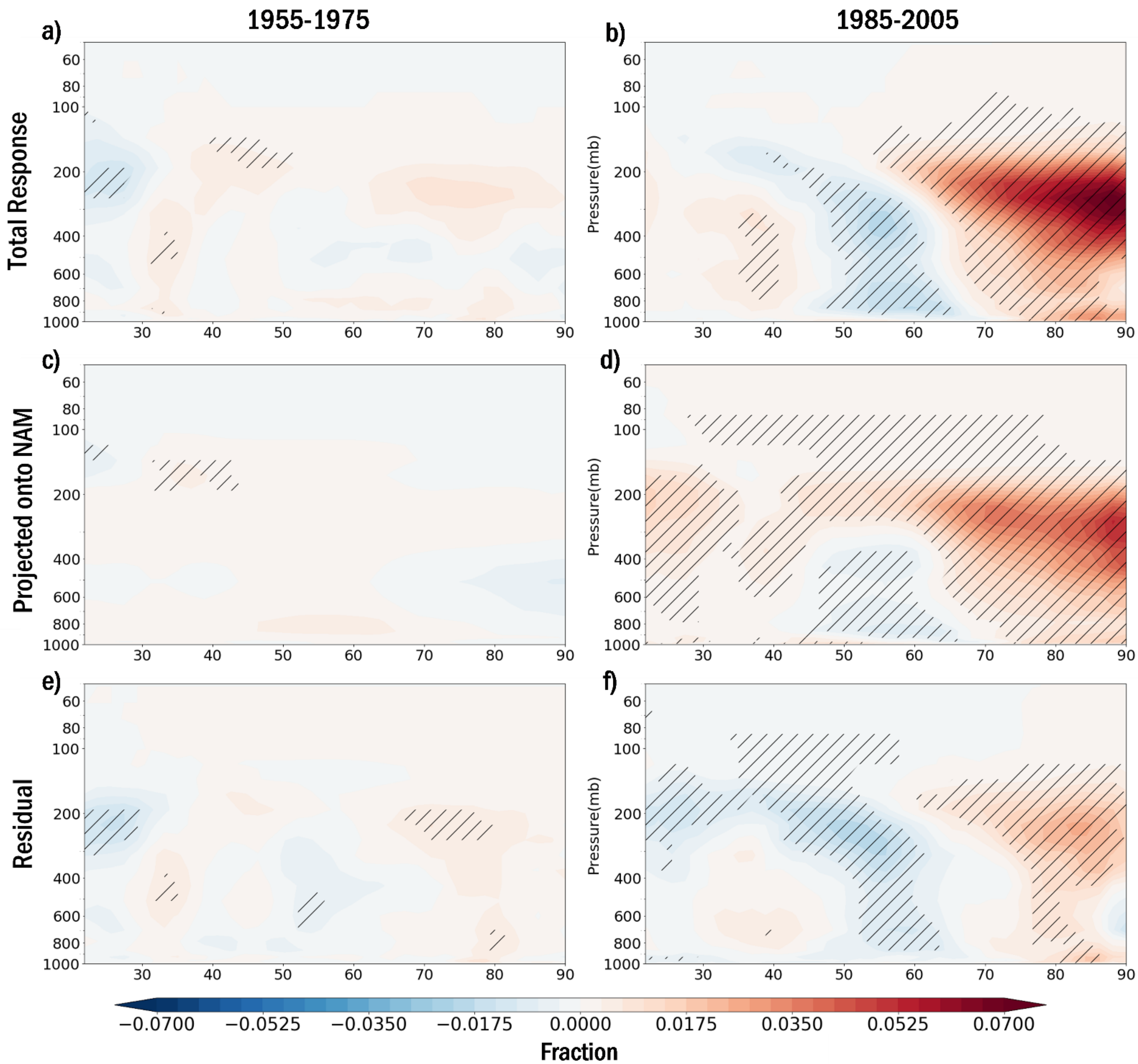

Figure 4. (a)-(b) Total April-May zonal mean cloud anomaly (low – high ozone years), (c)-(d) the projection of the anomaly onto the NAM, and (e)-(f) the residual for the (a), (c), (e) 1955-1975 and (b), (d), (f) 1985-2005 time periods. Hatching indicates regions of statistical significance at the 95% level.

Accepted for publication in *Journal of Climate*. DOI10.1175/JCLI-D-19-0867.1.

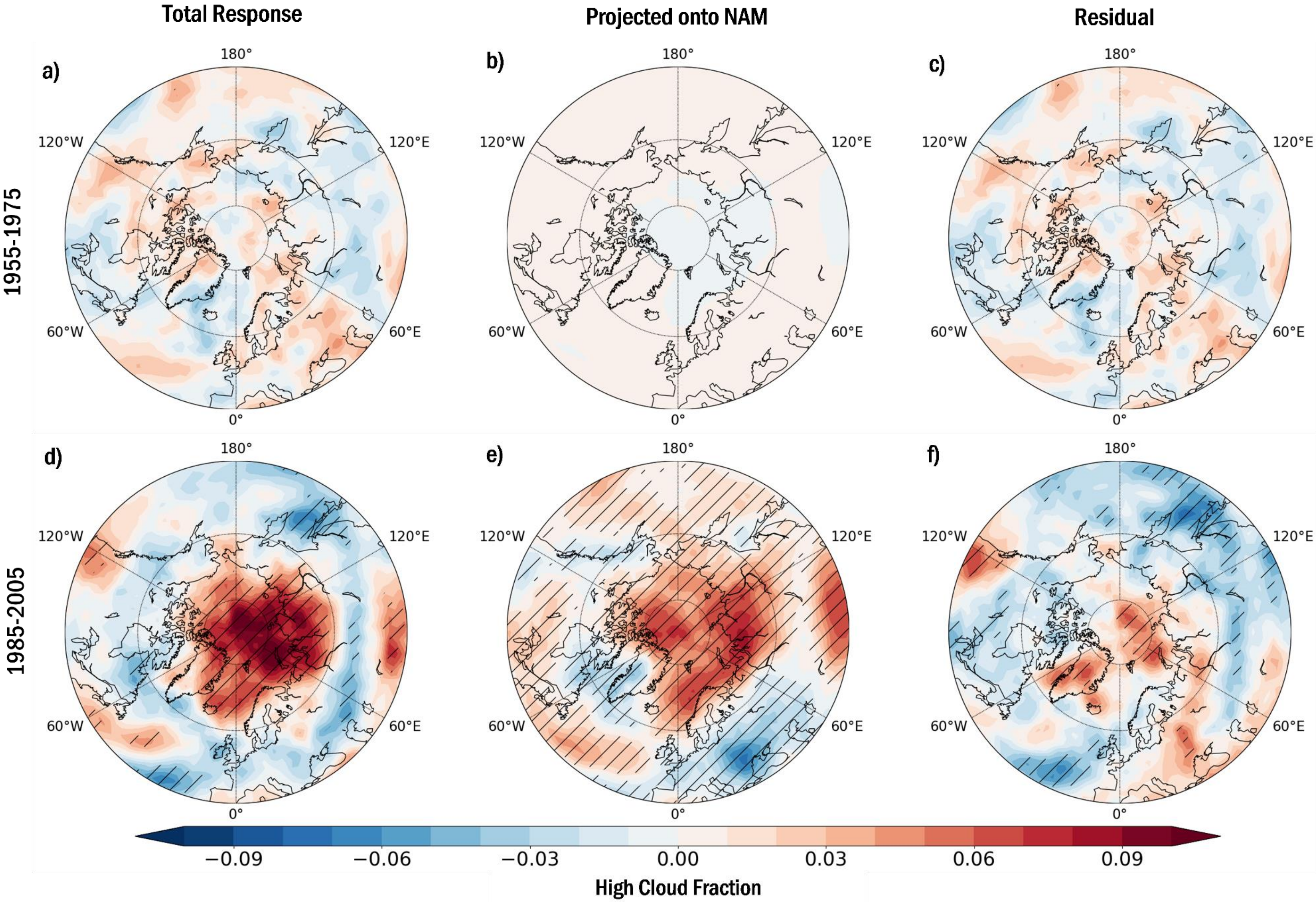

Figure 5. (a), (d) Total April-May high cloud anomaly (low – high ozone years), (b), (e) the projection of the anomaly onto the NAM, and (c), (f) the residual for the (a)-(c) 1955-1975 and (d)-(f) 1985-2005 time periods. Hatching indicates regions of statistical significance at the 95% level.

Accepted for publication in *Journal of Climate*. DOI10.1175/JCLI-D-19-0867.1.

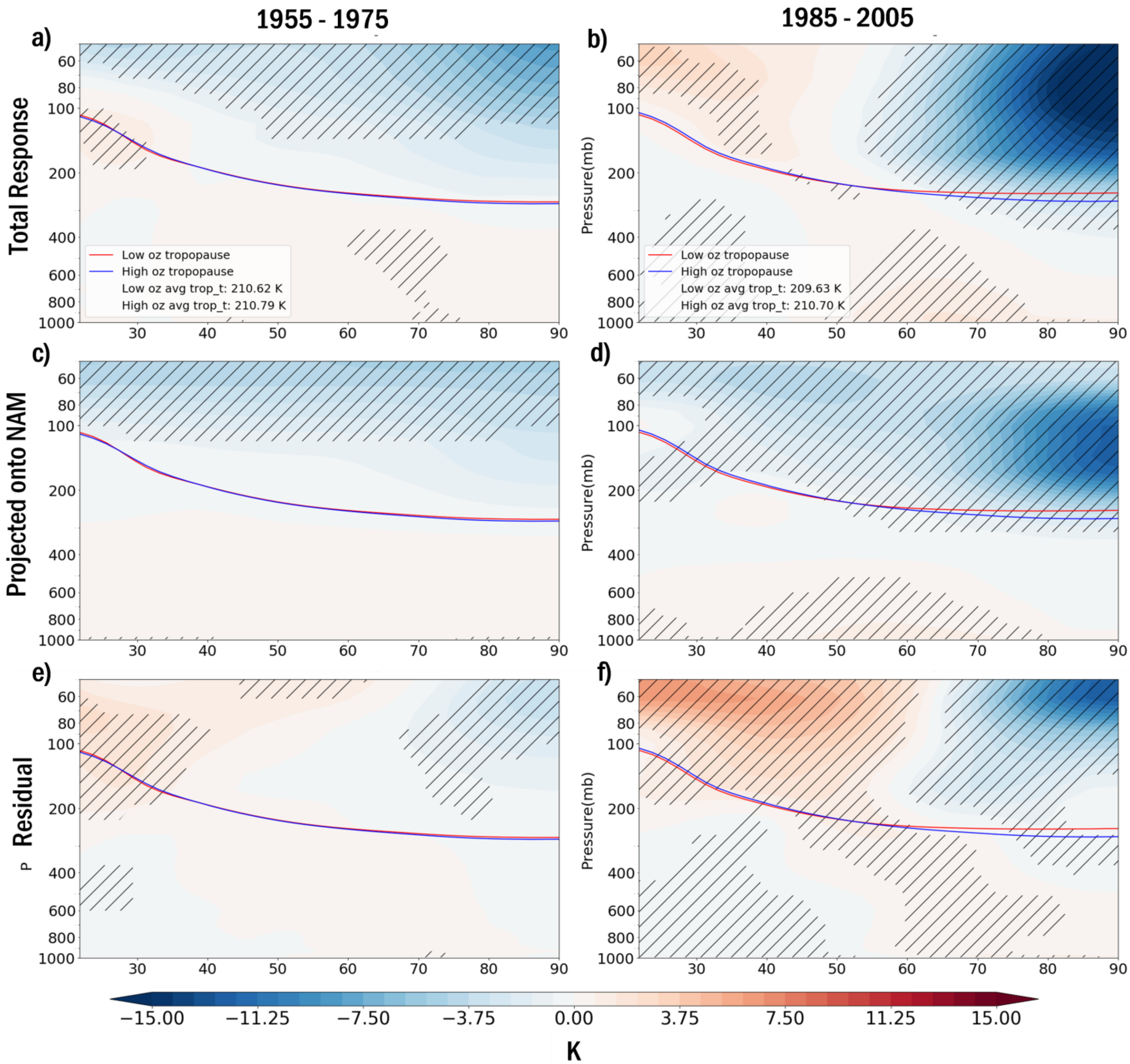

Accepted for publication in *Journal of Climate*. DOI10.1175/JCLI-D-19-0867.1.

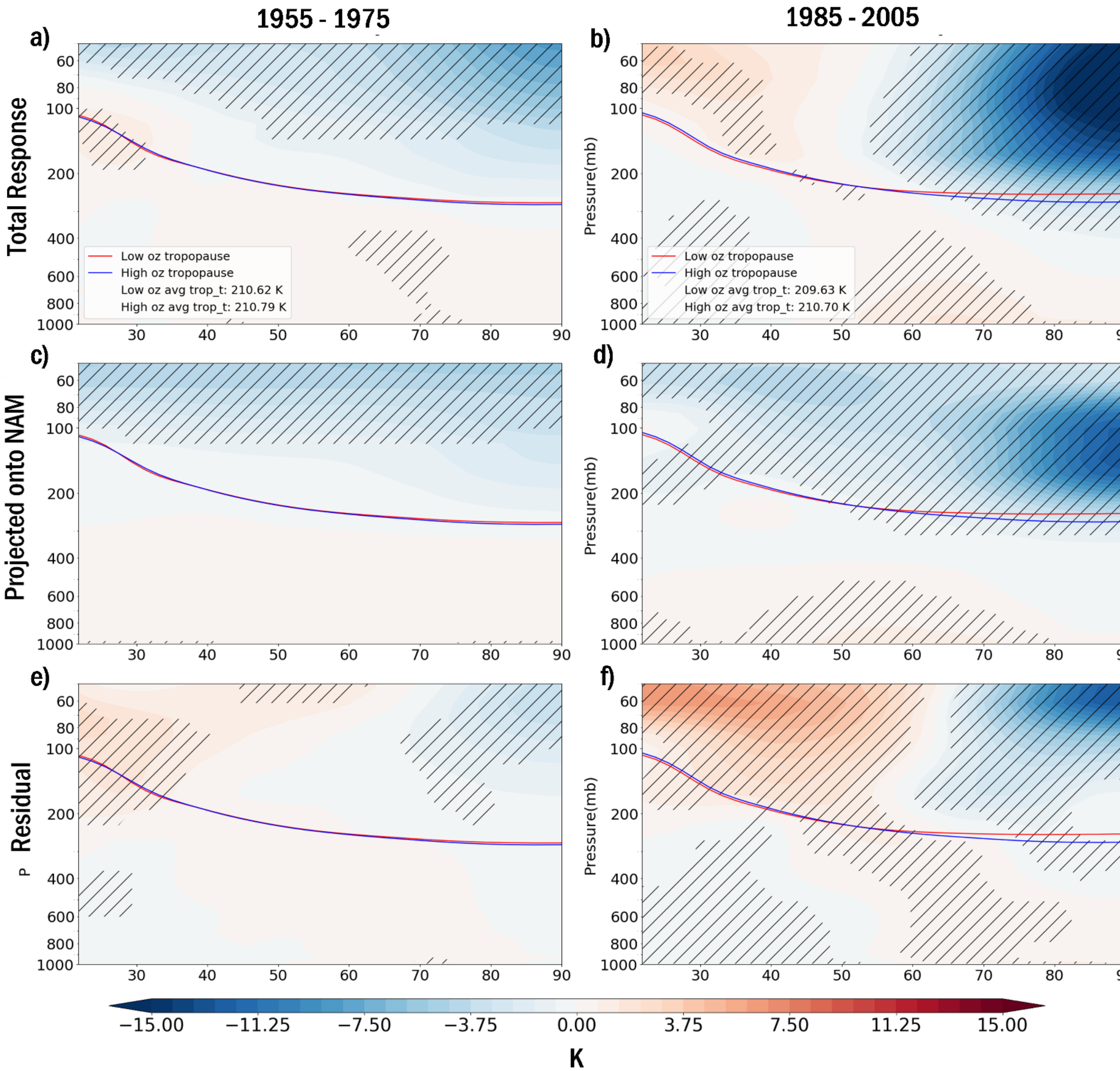

Figure 6. (a)-(b) Total April-May zonal mean potential temperature anomaly (low – high ozone years), (c)-(d) the projection of the anomaly onto the NAM, and (e)-(f) the residual for the (a), (c), (e) 1955-1975 and (b), (d), (f) 1985-2005 time periods. Hatching indicates regions of statistical significance at the 95% level.

Accepted for publication in *Journal of Climate*. DOI10.1175/JCLI-D-19-0867.1.

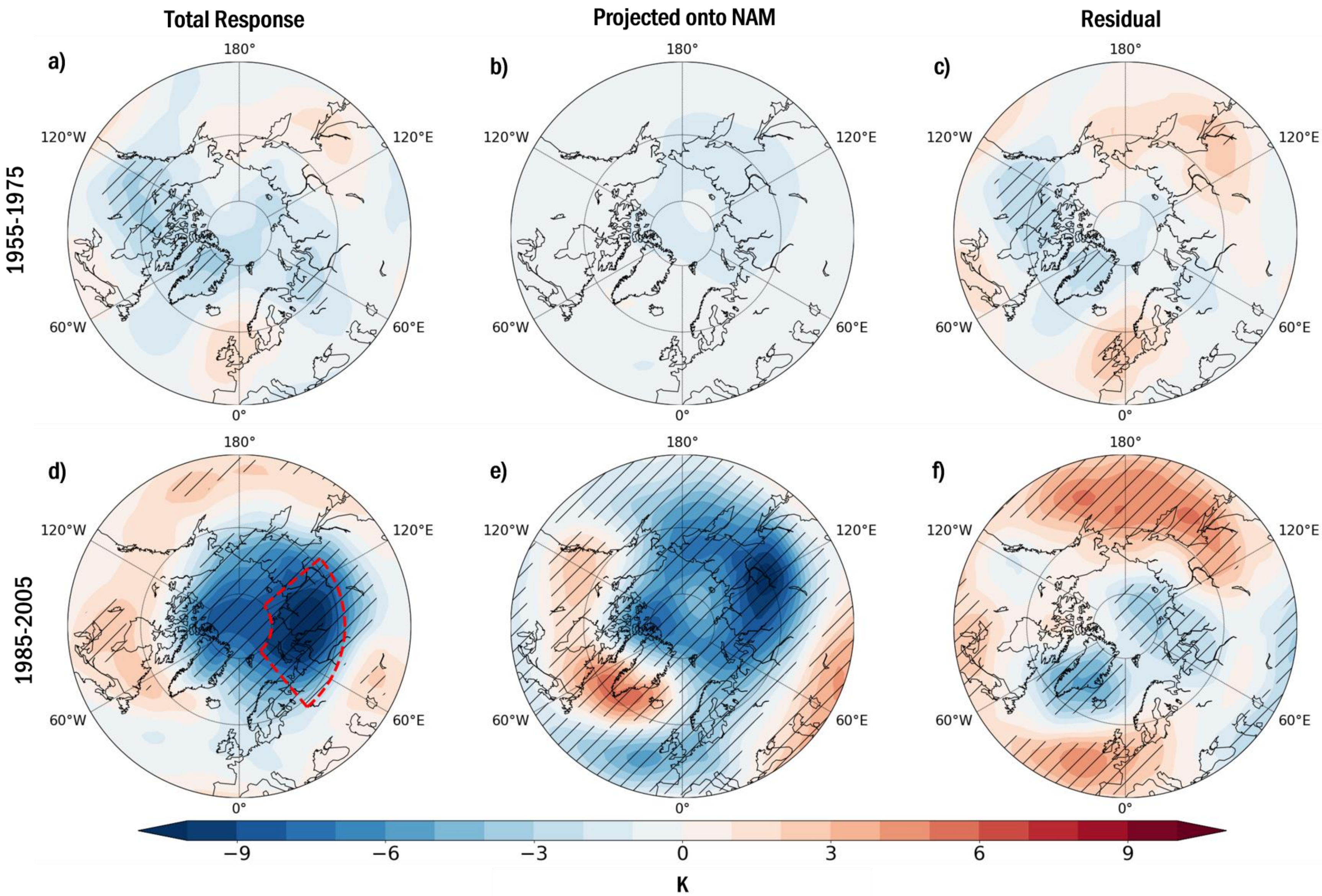

Accepted for publication in *Journal of Climate*. DOI10.1175/JCLI-D-19-0867.1.

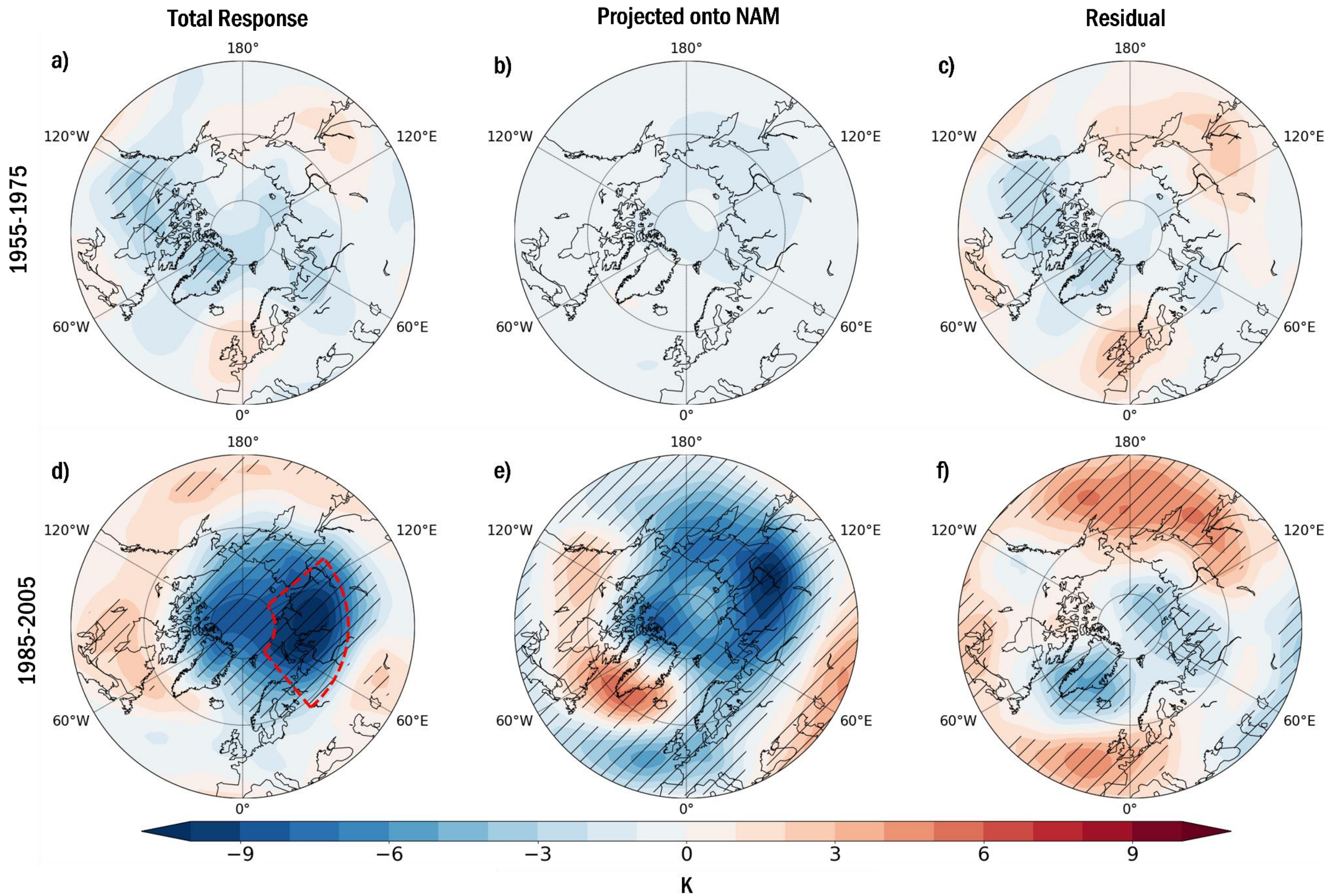

Figure 7. (a), (d) Total April-May upper tropospheric stability (UTS) anomaly (low – high ozone years), (b), (e) the projection of the anomaly onto the NAM and, (c), (f) the residcual for the (a)-(c) 1955-1975 and (d)-(f) 1985-2005 time periods. Hatching indicates regions of statistical significance at the 95% level .

Accepted for publication in *Journal of Climate*. DOI10.1175/JCLI-D-19-0867.1.

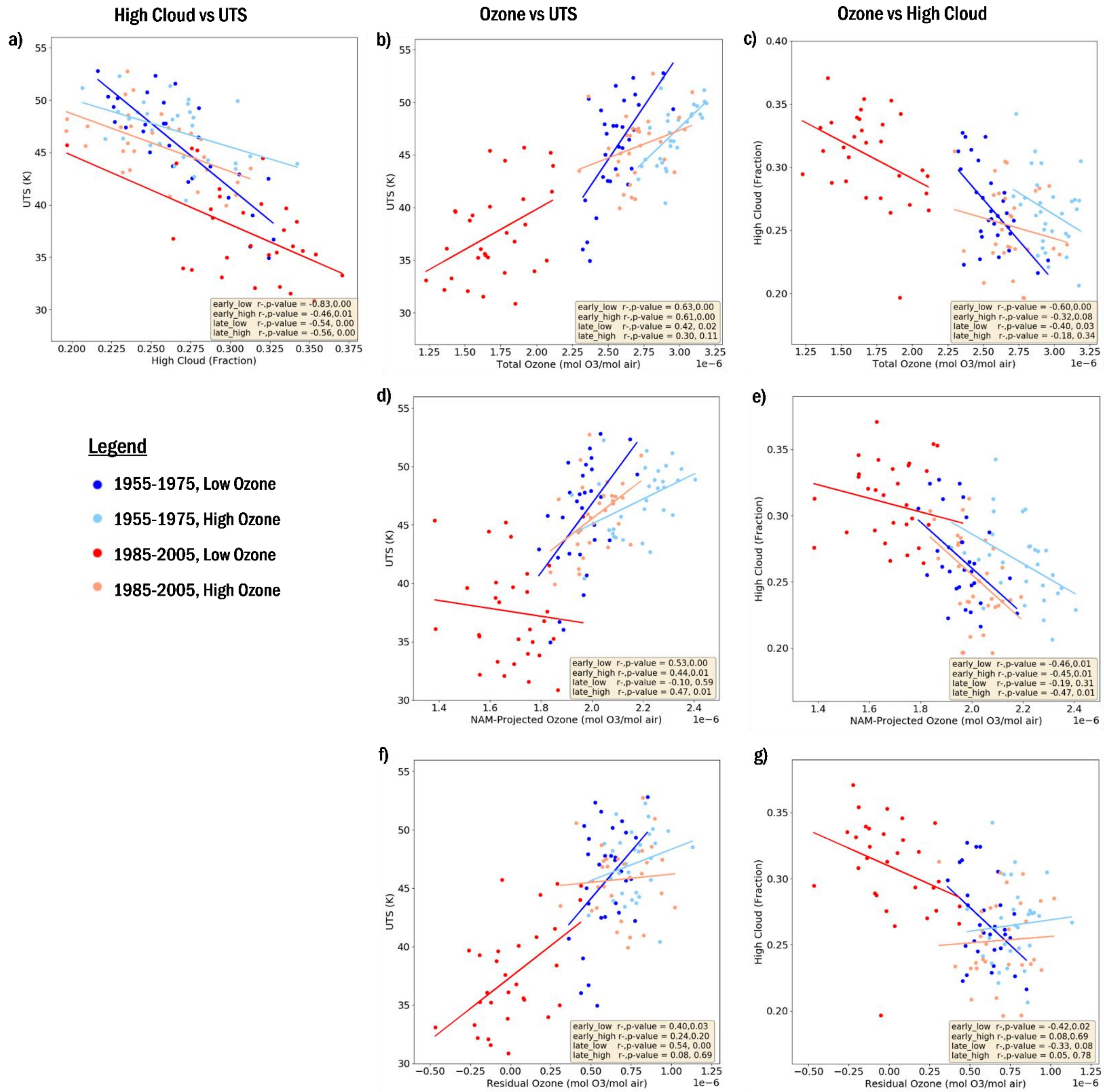

Figure 8. Scatter plots of (a) April-May high cloud and UTS, (b) April total ozone and April-May UTS, and (c) April total ozone and April-May high cloud for the northern Eurasia region (outlined in red in Figure 7d). Dark and light blue markers show the 1955-1975 (early) time period low and high ozone years, respectively and the red and orange markers show the 1985-2005 (late) time period low and high ozone years, respectively. (d) and (f) are NAM-projected and residual ozone (as in Figure 2) vs UTS, and (e) and (g) are NAM-projected and residual ozone vs. high cloud.

Accepted for publication in *Journal of Climate*. DOI10.1175/JCLI-D-19-0867.1.

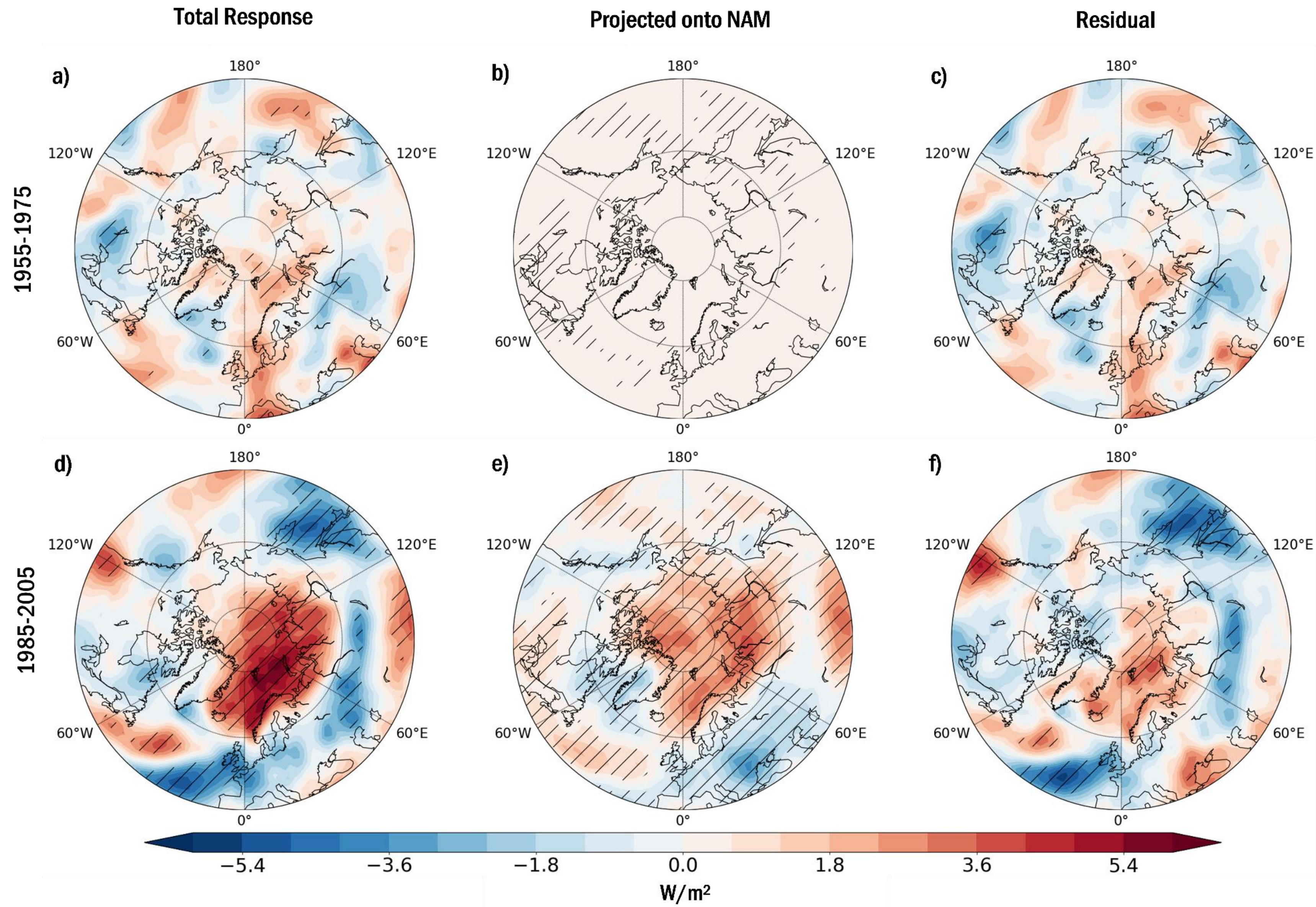

Figure 9. (a), (d) Total April-May top-of-atmosphere (TOA) long-wave (LW) adjusted cloud radiative effect anomalies (low – high ozone years), (b), (e) the projection of the anomaly onto the NAM and (c), (f) the residual for the (a)-(c) 1955-1975 and (d)-(f) 1985-2005 time periods. Hatching indicates regions of statistical significance at the 95% level.

Accepted for publication in *Journal of Climate*. DOI10.1175/JCLI-D-19-0867.1.

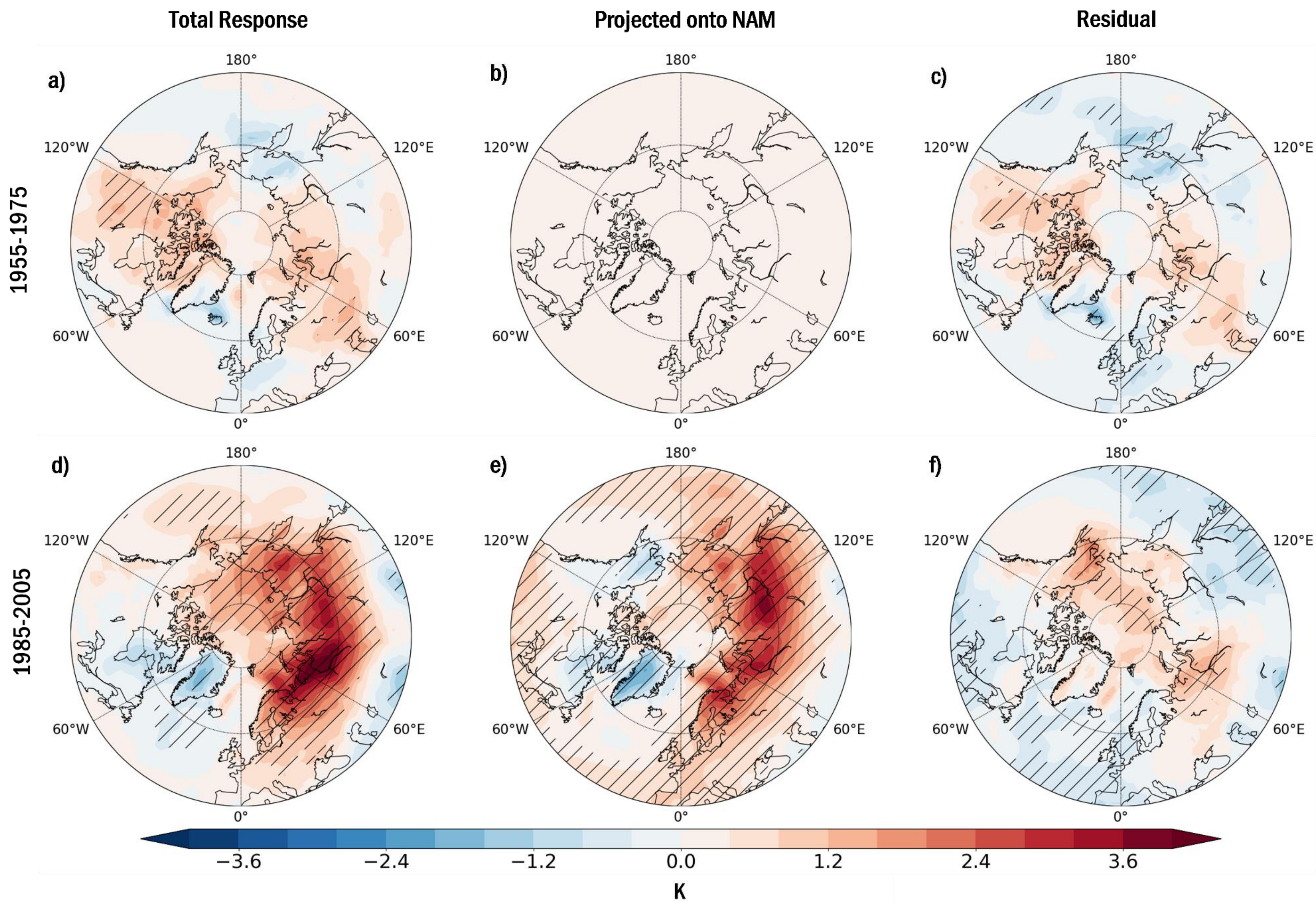

Figure 10. (a), (d) Total April-May surface temperature anomaly (low – high ozone years), (b), (e) the projection of the anomaly onto the NAM and (c), (f) the residual for the (a)-(c) 1955-1975 and (d)-(f) 1985-2005 time periods. Hatching indicates regions of statistical significance at the 95% level.

Accepted for publication in *Journal of Climate*. DOI10.1175/JCLI-D-19-0867.1.